Identification of Glycerol 3-phosphate acyltransferase as a potent modifier of α-Synuclein-induced toxicity

Kah Leong Lim

kahleong.lim@ntu.edu.sg

Lee Kong Chian School of Medicine, Nanyang Technological University, Singapore
https://orcid.org/0000-0002-5440-2588

Mengda Ren

Lee Kong Chian School of Medicine, Nanyang Technological University, Singapore

Gui Yin Grace Lim

Lee Kong Chian School of Medicine, Nanyang Technological University, Singapore

Willcyn Tang

Lee Kong Chian School of Medicine, Nanyang Technological University, Singapore

Article

Keywords: Parkinson's disease, lipid, glycerol 3-phosphate acyltransferase, GPAT, FSG67

Posted Date: April 9th, 2024

DOI: https://doi.org/10.21203/rs.3.rs-4199316/v1

Additional Declarations: There is **NO** Competing Interest.

Abstract

Although multiple cellular pathways have been implicated in a-Synuclein (a-syn)-associated Parkinson's disease (PD), the role of lipid metabolism remains elusive. Using the *Drosophila* system as a genetic screening tool, we identified *mino*, which encodes the mitochondrial isoform of the lipid synthesis enzyme glycerol 3-phosphate acyltransferase (GPAT), as a potent modifier of a-syn. Silencing the expression of *mino* significantly suppresses a-syn-induced PD phenotypes in *Drosophila*, including dopaminergic neuronal loss and locomotion defects as well as circadian rhythm-related activities, whereas *mino* overexpression yields opposite effects. Mechanistically, we found that *mino* modulates the levels of mitochondrial reactive oxygen speciesand lipid peroxidation. Importantly, treatment of a-syn-expressing flies with FSG67, a GPAT inhibitor, reproduces the benefits of *mino* knockdown. FSG67 also inhibited a-syn aggregation and lipid peroxidation in mouse primary neurons transfected with a-syn preformed fibrils. Our study elucidates an important factor contributing to a-syn toxicity and offers a novel therapeutic direction for PD.

HIGHLIGHTS

- *Drosophila* screen identifies *mino* (glycerol 3-phosphate acyltransferase) as a novel modifier of a-Synuclein (a-syn)
- Silencing of *mino* expression abrogates the pathological phenotypes in flies induced by elevated levels of a-syn.
- Silencing the expression of other GPAT similarly produces beneficial outcomes in a-syn flies, suggesting a common role of GPAT in modulating a-syn neurotoxicity.
- Pharmacological inhibition of GPAT via FSG67 treatment inhibits a-syn aggregation and lipid peroxidation in both fly brains and mouse primary neurons.

INTRODUCTION

Parkinson's disease (PD) is a prevalent neurodegenerative disease that is characterized clinically by a constellation of motoric deficits including bradykinesia, tremors, and rigidity. The principal neuropathology underlying PD is the loss of dopaminergic (DA) neurons in the substantia nigra pars compacta of the midbrain, which results in the disruption of the nigrostriatal pathway leading to movement disorders. Accompanying the DA neurodegeneration is the presence of intraneuronal inclusions known as Lewy bodies (LBs), which are enriched with the presynaptic protein α-syn [1,2].

Notably, rare mutations and copy number variations in the α-syn-encoding gene *SNCA*, such as A30P and A53T, are causative of monogenic forms of PD [3–5]. Further, genome-wide association studies have also implicated genetic variations of *SNCA* increasing the risk for idiopathic PD [6]. However, the effects of these genetic variations are modest compared to other PD risk genes, like *Gba1* or *LRRK2* [7], potentially attributable to the polygenetic mode of inheritance and genetic modifiers' interaction with *SNCA* [8,9].

Interestingly, a recent retrospective analysis of studies on α-syn revealed interactions with up to 365 genetic modifiers, underscoring α-syn's intricate involvement in PD pathology [10]. These modifiers are linked to diverse biological pathways, including mitochondrial function, antioxidant/glutathione metabolism, autophagy, protein degradation, vesicle trafficking, neuroinflammation, cytoskeleton dynamics, and lipid metabolism. In particular, the role of lipid dyshomeostasis in the development of PD has gained much attention in recent years. LBs, traditionally seen as comprised mainly of α-syn, is now recognized to be a complex mixture of protein aggregates intertwined with lipid components including from damaged mitochondria, autophagosomes, lysosomes, and fragments of lipid membranes, emphasizing the pivotal role of lipids in the biogenesis of LB associated with PD pathogenesis [11,12]. Furthermore, several genes linked to PD, such as *PLA2G6*, *GBA*, *LRRK2*, *Parkin*, *SMPD1*, *SCARB2*, *DGKQ* and *SYNJ1*, play important roles in lipid metabolism [13–15]. Not surprisingly, lipidomic irregularities are observed in the serum and brain tissues of PD patients, including elevated levels of polyunsaturated fatty acids (PUFAs), glycerophosphatidylcholine, diacylglycerol, and triglycerides [14,16–18].

α-syn is known to interact with lipids and its aberrations disrupts this interaction. Disease-related mutations in α-syn, such as A30P, E46K, and G51D, all of which are clustered in the protein's N-terminus, alter its affinity for lipid membranes and influence the balance between its multimeric and monomeric states [19–21]. α-syn deficiency can lead to changes in palmitate uptake and brain neutral lipid content, affecting the acylation of arachidonic acid and docosahexaenoic acid, and their conversion into phospholipid pools [22–24]. Conversely, excessive α-syn induces the accumulation of lipid droplets in yeast [25], and promotes the synthesis of polyunsaturated ether phospholipids in iPSC-derived human midbrain dopaminergic neurons, leading to lipid peroxidation and increased sensitivity to ferroptosis, a form of cell death marked by iron-dependent accumulation of lipid peroxides [26]. α-syn also contributes to ferroptosis by generating lipid peroxidation [27].

Various lipid-metabolizing enzymes are known to affect α-syn aggregation and associated neurotoxicity. For example, stearoyl-CoA desaturase (SCD) regulate the unsaturation level of fatty acids and affect α-syn oligomeric composition in yeast, cells and transgenic mice [28–32]; Fatty acid CoA synthetase long-chain family member 4 (ACSL4) regulates fatty acids partitioning into the fatty acyl-CoA pool and influences lipid peroxidation and ferroptosis that are linked to α-syn-induced neurotoxicity [26,33,34]. Lysophosphatidic acid acyltransferase (LPACT), which converts lysophospholipids to phospholipids and helps to reconstitute phosphatidylcholine, is upregulated in postmortem PD brains and cultured neurons overexpressing *SNCA* E35K/E46K/E61K mutants [35]. Finally, LIPE, the rate-limiting lipase enzyme, regulates α-syn tetramer:monomer equilibrium and α-syn neurotoxicity [36]. Accordingly, modulating fatty acid and lipid metabolism genes, including *LPCAT*, *SCD* and *LIPE*, may reverse α-syn aggregation and associated phenotypes, which was observed in several PD models [30,35,36]. Furthermore, YTX-7739, an SCD inhibitor, has progressed to phase 1 clinical trials [29]. Taken together, it is important to clarify the role of lipids in the pathogenesis of PD that holds promise to shed light on novel therapeutic directions for PD treatment.

Using transgenic *Drosophila* overexpressing α-syn as a model for genetic screening, we report here the identification of *mino*, which encodes the mitochondrial isoform of the lipid synthesis enzyme glycerol 3-phosphate acyltransferase (GPAT), as a potent modifier of α-syn. We find that siRNA-mediated silencing of *mino* expression significantly mitigates α-syn-induced PD phenotypes in *Drosophila*, including dopaminergic neuronal loss and associated locomotion defects as well as circadian rhythm-related activities, whereas overexpression of yields opposite effects. The beneficial effects of *mino* silencing on α-syn-expressing flies are linked to reduced levels of mitochondrial reactive oxygen species and lipid peroxidation. Additionally, we extend our investigation to include the predicted endoplasmic reticulum-localized GPAT (*CG15450* and *Gpat4*) and the related gene *Gnpat*, that encodes peroxisome-localized glyceronephosphate O-acyltransferase. Knocking down *Gpat4*, or *CG15450* similarly reduces α-syn aggregation and suppresses α-syn neurotoxicity, suggesting a common role of GPAT in modulating α-syn neurotoxicity. Consistent with this, treatment of α-syn-expressing flies with FSG67, a GPAT inhibitor, reproduces the benefits of *mino*/GPAT knockdown. Notably, FSG67 also inhibits α-syn aggregation and lipid peroxidation in mouse primary neurons transfected with α-syn preformed fibrils. Taken together, our study elucidates an important factor/pathway contributing to α-syn toxicity and offers a novel therapeutic direction for PD.

RESULTS

Drosophila screen identifies mino RNAi as a suppressor of α-syn neurotoxicity

To identify modifiers of α-syn, we performed a genetic screen in a *Drosophila* model of synucleinopathy, where we overexpressed human wild-type α-syn in the photoreceptor (PR) neurons R1-R6. Overexpression of α-syn in PR neurons is known to induce vacuole formation in the lamina layer, where PR neurons form synapses with downstream lamina monopolar neurons [37], which offers a convenient readout. To identify candidate genes for screening, we utilized a predictive model deltaSVM to analyze a collection of SNPs dataset on the Parkinson's disease genome-wide association study locus browser (v1.9) from 83 human PD risk loci that may confer differential transcription factor binding [38,39]. Based on the SNP locations, we manually selected 1–3 nearest genes for each locus. Subsequently, we identified available RNAi or dCas9/gRNA-VPR overexpression lines from the Bloomington *Drosophila* Stock Center (BDSC). These lines targeted the *Drosophila* orthologues of the selected human genes, which were identified using the DIOPT Ortholog Finder [40]. Finally, we crossed 107 lines targeting 92 genes with the *Drosophila* synucleinopathy model to examine whether they can influence α-syn-induced vacuole formation in the lamina [41] (**Supplementary Data 1**).

From the above pool of 107 RNAi and overexpression fly lines, we found 5 RNAi lines (targeting *Ggamma1*, *mino*, *nonC*, *RpII215* or *Src64B*) and 9 overexpression lines (targeting *Acbp1*, *Bap170*, *bnl*, *CG5214*, *CG7461*, *Psn*, *Pu*, *SdhC*, andor *wg*) that suppress vacuole formation in α-syn flies by more than 2-fold at an adjusted *p*-value of 0.01 (Fig. 1A). We subsequently selected four lines whose targeted genes are associated with energy and lipid metabolism, i.e. *mino*, *CG5214*, *CG7461*, *SdhC*, to test if their RNAi or overexpression could rescue the decline in climbing abilities induced by α-syn (**Supplementary Fig. 1A**).

Among these, we found that *mino* RNAi expression in α-syn flies (*nSyb-GAL4/+; UAS-SNCA.J7/+;*) is the only one that could alleviate their climbing phenotype for up to 8 weeks post-eclosion (Fig. 1B). This phenomenon is similarly observed when we employed another fly synucleinopathy model expressing α-syn in a pan-neuronal manner (*nSyb-QF2 QUAS-SNCA/+*) that triggers more severe phenotype (Fig. 1C). Conversely, overexpressing *mino* using an upstream *UAS* insertion mutant *EY00734* exacerbates α-syn-induced loss of locomotor abilities (Fig. 1C). Collectively, these results underscore *mino*'s role in modulating α-syn neurotoxicity. As due diligence, we also ascertained the expression of *mino* in both the RNAi and overexpression lines using qPCR of brain-extracted mRNAs (**Supplementary Fig. 1B**).

Pan-neuronal overexpression of α-syn is known to be toxic to DA neurons [42]. Among the clusters of DA neurons in the fly brain, the protocerebral anterior medial (PAM) cluster is one of the largest clusters that contain more than 100 tyrosine hydroxylase (TH)-positive DA neurons. PAM cluster is involved in startle-induced negative geotaxis [43,44]. To investigate the role of *mino* in modulating α-syn-induced DA neurodegeneration, we utilized the Labkit pixel classification method to automatically quantify the PAM dopamine neuron cluster (Fig. 1D and 1E, **Supplementary Fig. 1E**) [45]. In the first group of α-syn mutant flies (*nSyb-GAL4/+; UAS-SNCA.J7/+;*) tested, we observed a significant decrease in PAM TH + cells at day 49, but not day 32, post-eclosion, when compared to *nSyb-GAL4/+* control flies. Nonetheless, we found that the observed neuronal loss is rescued in the presence of *mino* RNAi (Fig. 1D). In the second group of α-syn mutant flies that has more severe phenotype, a decline in TH + cells is already evident at day 32 post-eclosion compared to their nSyb-QF2/+ control counterparts. Again, *mino* RNAi mitigates the neurodegeneration, although more modestly so (**Supplementary Fig. 1C**). The beneficial effects of *mino* RNAi persisted when we elevated the housing temperature to 29°C, which enhances the expression of both α-syn and *mino* RNAi (Fig. 1F). As expected, *mino* overexpression triggers the opposite effects, i.e. it exacerbates the loss of TH + cells in α-syn flies (Fig. 1F). Although α-syn expression alone resulted in an overall decrease in TH + cells during the pre-adult stage, we ascertained that *mino*'s impact on α-syn-associated neurodegeneration is manifested at the adult but not pre-adult stage, as evidenced by the absence of significant differences in TH + cells in α-syn flies at day 1 post-eclosion in the presence of *mino* RNAi or overexpression (**Supplementary Fig. 1D**). Thus, *mino* is likely acting on α-syn-related pathways in a post-developmental fashion.

Studies on α-syn PD models have revealed disruptions in circadian rhythm-linked locomotor behavior [46–48], which may reflect sleep disturbances in human PD. Consistent with these studies, we found that α-syn expression in flies induces an age-dependent decline in their daily activities, i.e. the disappearance of the morning peak during the dark-light transition and a reduced amplitude at the evening peak at the light-dark transition (Fig. 2A and 2B). This disruption in the circadian rhythm-related locomotor activities in α-syn is alleviated in the presence of *mjno* RNAi (Fig. 2A and 2B). However, although *mino* RNAi restored the evening peak's average intensity, it did not lead to the recovery of the morning peak (Fig. 2C-E). In contrast, *mino* overexpression tends to aggravate α-syn-induced reduction of the evening peak (Fig. 2A-E). In the absence of α-syn expression, neither *mino* RNAi nor its overexpression affects the daily total activities of *Drosophila* (Fig. 2A-E).

We recognize that the metabolic crosstalk between neurons and glia significantly influences neuronal energy balance. To investigate whether the modifying effects of *mino* on α-syn operates selectively in neurons or extends to glial cells, we downregulated *mino* expression either solely in glia (with *repo-GAL4*) or simultaneously in neurons and glia (with *nSyb-GAL4 and repo-GAL4*) and assessed their impact on the fly's daily locomotor activities. We found that expressing *mino* RNAi in glia alone has no credible α-syn-modifying effects whereas simultaneous *mino* RNAi expression in neurons and glia mitigates the decline in daily locomotor activities exhibited by α-syn flies (**Supplementary Fig. 2A and 2B**). Thus, *mino* seems to exert its effects on α-syn in a cell-autonomous fashion.

Taken together, our results identified *mino* as a novel modifier of α-syn whose downregulation can alleviate α-syn-induced phenotypes in two distinct *Drosophila* models of α-syn-associated PD.

mino modulates α-syn-induced lipid peroxidation, 4-HNE accumulation and associated cell death

α-syn neurotoxicity is associated with alterations in lipid profiles, elevated lipid peroxidation and sensitivity towards ferroptosis [17,26,27,49,50]. Given that mino facilitates the acylation of acyl-CoA to glycerol-3-phosphate, a pivotal step in synthesizing phospholipids and triglycerides, we were curious to examine whether *mino* could impact on α-syn-associated lipid peroxidation. To investigate this, we labeled neuronal membranes with a cell membrane-localized infrared fluorescent protein (mIFP) whose pan-neuronal expression is directed by *nSyb-GAL4* [51], and used BODIPY C11 lipid dye to analyze lipid peroxidation levels. Under standard culture conditions (25°C for 3 weeks), we observed that α-syn expression did not appreciably alter neuronal membrane lipid peroxidation levels, although the extent of lipid peroxidation decreased in the presence of *mino* RNAi and increased when *mino* is overexpressed (Fig. 3A, 3B and 3C). In the absence of α-syn expression, neither *mino* RNAi nor its overexpression alone affects the basal lipid peroxidation level (Fig. 3C). When flies were raised at 29°C for 3 weeks, α-syn overexpression alone significantly elevated the level of lipid peroxidation in neuronal membranes (Fig. 3A and 3C). This elevated lipid peroxidation level is significantly blunted by *mino* RNAi expression but becomes aggravated in the presence of *mino* overexpression (Fig. 3C). As lipid peroxidation promotes the buildup of products such as 4-hydroxynonenal (4-HNE) and malondialdehyde (MDA), we probed and found an elevated presence of the lipid peroxidation product 4-HNE in α-syn-expressing fly brains (Fig. 3D and 3E). As expected, the observed 4-HNE level is suppressed in the presence of *mino* RNAi expression and enhanced when *mino* is overexpressed (Fig. 3D and 3E).

Next, we investigated whether mino's effects on α-syn-induced lipid peroxidation correlates with changes in cell death. By means of TUNEL assay, we found that α-syn expression results in marked cell death compared to its control counterparts, especially at week 2 and 3 but not appreciably at earlier timepoints (day 1 and week 1) post-eclosion (Fig. 3F, 3G, **and Supplementary Fig. 3A**). Consistent with the results above, α-syn-induced cell death is significantly reduced in the presence of *mino* RNAi and aggravated when *mino* is overexpressed (Fig. 3F, 3G, **and Supplementary Fig. 3A**). Neither *mino* RNAi or its overexpression alone induces significant cell death in flies (Fig. 3F, 3G, **and Supplementary Fig. 3A**). To distinguish between apoptotic and non-apoptotic event, we co-stained the brains with cleaved caspase-3

antibody but did not detect positive staining (Fig. 3F). To confirm the antibody's efficacy, we stained *hs-hid* (*heat shock- head involution defective*) third instar larva brain (which expresses hid upon heat shock) after a 2-hours heat shock at 37°C and observed the expected strong positive staining (**Supplementary Fig. 3B**). Despite the possibility that cleaved caspase-3 might be detectable only during specific stages of apoptosis, the absence of its staining at weeks 2 and 3 in α-syn flies suggests that apoptosis may not be primarily occurring in α-syn-expressing fly brains.

A common role of GPAT as modulators of α-syn neurotoxicity

mino encodes an enzyme that belongs to the conserved *GPAT* gene family that are responsible for catalyzing the initial acylation step in the *de novo* synthesis of phospholipid [52]. This prompted us to examine whether other *GPAT* members may play similar roles to *mino* in modulating α-syn neurotoxicity. To address this, we extended our RNAi targeting to include two other *Drosophila* homologs of *GPAT*, i.e. *Gpat4*, and *CG15450*. Whereas mino is predicted to reside on the mitochondria, the product of both *Gpat4*, and *CG15450* are predicted to reside on the ER [53]. Similar to *mino* RNAi, downregulation of the expression of *Gpat4*, and *CG15450* effectively suppresses the decline in startle-induced climbing abilities (Fig. 4A) and also mitigates the reduction in daily locomotor activities in α-syn flies (Fig. 4B and 4C). Aligning with these observations, *Gpat4*, and *CG15450* RNAi expression also attenuates the decline of DA neuronal number in the PAM cluster induced by α-syn (Fig. 4D). Further supporting a common role for GPAT in modulating α-syn-induced toxicity, we found that when α-syn flies were treated with the GPAT inhibitor FSG67 [54], they showed improvement in their daily locomotor activities (Fig. 4E and 4F). In contrast, RNAi-mediated silencing of Gnpat expression, a related enzyme predicted to reside on the peroxisome that is responsible for catalyzing the initial acylation step of ether lipid synthesis, did not significantly affect the locomotion activities of α-syn flies (Fig. 4A-C). Surprisingly, *Gnpat* RNAi reduces the loss of DA neurons in the PAM cluster (Fig. 4D). Despite this unexpected finding, these results collectively highlight *mino* as a representative of the broader GPAT activity responsible for modulating α-syn neurotoxicity.

GPAT RNAi suppresses α-syn higher-order oligomers formation and mitochondrial ROS accumulation

We have previously demonstrated that α-syn expression in the *Drosophila* brain leads to a metabolic shift from oxidative phosphorylation to glycolysis, a phenomenon that is regulated by hypoxia-inducible factor HIF1A and the kinase module component of the mediator complex Med13 [41]. We were curious whether *mino* would influence this metabolic reprogramming induced by α-syn. Unlike HIF1A and Med13, we did not observe significant alterations in the α-syn-induced increase of glycolysis enzymes Pgi and Ldh in the presence of *mino* RNAi or other GPAT RNAi tested (Fig. 5A). Moreover, we found no credible evidence of changes in the total α-syn level upon *mino*/GPAT RNAi co-expression, suggesting that *mino* is likely

exerting its effects downstream of α-syn, potentially impacting on α-syn aggregation and associated mitochondria-related oxidative stress level.

Several studies have highlighted the involvement of phospholipid membranes and cardiolipin, a mitochondrial lipid, in initiating the early stages of α-syn misfolding and aggregation [55,56]. Given that GPAT catalyzes crucial early steps in glycerolipid synthesis, we investigated whether GPAT influences the formation of α-syn oligomers/aggregates. In contrast to many α-syn-based PD models employing mammalian cells, α-syn expressed in the *Drosophila* brains is predominantly detected as monomers in both soluble and insoluble fractions [42,57]. However, oligomeric species of α-syn can be revealed through removing Triton X-100 and DTT from buffers while using cross-linkers like Dimethyl dithiobispropionimidate (DTBP) [58]. Supporting this, we observed that α-syn oligomers can indeed be stabilized in DTT- and Triton X-100-free buffers; the levels of which increases with increasing DTBP concentrations of up to 5 mmol, thereafter a sharp decline follows (**Supplementary Fig. 4A and 4B**). Using this method of detection for α-syn oligomers, we found that *mino/*GPAT RNAi, but not *Gnpat* RNAi, suppress the formation of higher-order α-syn oligomers in the presence of 4 mmol DTBP (Fig. 5B and 5C). Interestingly, *GPAT* RNAi specifically reduces α-syn tetramers and higher-order oligomers, without impacting α-syn dimers or trimers, either in comparison to their respective monomers or in total α-syn levels (Fig. 5B and 5C).

The formation of α-syn oligomers and aggregates is known to correlate with the generation of mitochondrial reactive oxygen species (ROS) including H_2O_2 [55]. To assess mitochondrial H_2O_2 levels, we utilized the fluorescent H_2O_2 sensor mito-roGFP2-Orp1 [59]. Although *mino* RNAi or overexpression did not significantly affect the mitochondrial H_2O_2 index in the absence of α-syn, their effects are evident in α-syn-expressing neurons, where *mino* RNAi results in a significant reduction of the H_2O_2 index, whereas *mino* overexpression exacerbates it (Fig. 5D and 5E). Alongside this, we employed MitoTimer, a sensor that reflects the cumulative redox history of mitochondria, to examine mitochondria maturation in these flies [60]. We observed a dramatically accelerated mitochondria maturation process in wild-type brains expressing α-syn, a phenomenon that is mitigated by *mino* RNAi (Fig. 5F and 5G). We also noted a minor suppression of mitochondria maturation by *mino* RNAi in the absence of α-syn (Fig. 5F and 5G).

Taken together, our results above revealed a connection between GPAT and the formation of α-syn oligomers and associated mitochondrial maturation/H_2O_2 generation, an important link that was not previously reported that may have pathophysiological relevance to α-syn-related PD pathogenesis.

Pharmacological inhibition of GPAT suppresses α-syn-induced lipid peroxidation in mouse primary neurons treated with α-syn preformed fibrils (PFF)

To examine the relevance of our findings above in the mammalian context, we investigated whether GPAT inhibition could similarly retard the formation of pathological α-syn species and the events they trigger in primary mouse neurons. To address this, we treated primary mouse neurons with α-syn preformed fibrils (PFF). In the presence of PFF treatment, we observed the appearance of elongated α-syn fibers that stain

prominently with antibody against α-syn phosphorylation at serine 129 (pS129) (Fig. 6A and 6B). These phosphorylated α-syn fibers form dense clusters in both neurites and cell bodies of the PFF-treated neurons (Fig. 6A and 6B). Neither such morphology nor pS129 α-syn staining was observed when the primary neurons were treated with α-syn monomers (Fig. 6A and 6B). Importantly, co-treatment of neurons with PFF and the GPAT inhibitor FSG67 significantly attenuated the formation of p129 α-syn fibers and clusters (Fig. 6A and 6B).

Interestingly, PFF-induced pS129 fiber/aggregation colocalizes with the lipid peroxidation product 4-HNE and PFF-treated neurons exhibit elevated levels of both 4-HNE and MDA (Fig. 6A and 6B). Moreover, these neurons show excessive BODIPY 488 background staining, which is absent in in mock or monomers-treated neurons, suggesting the presence of lipid-related abnormalities in PFF-treated neurons. These molecular phenotypes induced in neurons by α-syn are all ameliorated in the presence of FSG67 co-treatment (Fig. 6A and 6B). Finally, we also stain PFF-treated neurons with BODIPY C11 to detect for lipid peroxidation. As expected, neurons treated with PFF, but not α-syn monomers, exhibit enhanced lipid peroxidation levels that are significantly reduced when they are co-treated with FSG67 (Fig. 6C).

Collectively, our results suggest that GPAT are also key players in α-syn-induced cytotoxicity in the mammalian context and that their modulation would similarly offer benefits.

DISCUSSION

In this study, we identified *mino*, alongside members of the GPAT family, as novel genetic modifiers of α-syn-induced neurotoxicity. Using both *Drosophila* and primary mouse neuronal model of synucleinopathy, we demonstrated that pharmacological or genetic reduction of *mino*/GPAT activity effectively mitigates α-syn-associated pathological phenotypes that includes a reduction in the neuronal lipid peroxidation level. These new insights that we have provided in this report support a key role for lipid-related pathways in the pathogenesis of PD and therein offers a therapeutic angle focused on lipid aberrations in PD.

α-syn comprises of an amphipathic N-terminal region, a hydrophobic non-amyloid-component (NAC) domain, and an acidic C-terminal domain. The N-terminal and NAC regions house multiple lipid membrane binding motifs critical for the protein's interaction with lipid membranes [19,61]. α-syn aggregation is enhanced in the presence of phospholipid surfaces [62–64] and its toxicity can also be altered by the saturation level of fatty acids [28]. In turn, α-syn can trigger various lipid abnormalities including variations in neutral and polar lipid levels, ester and ether lipids, unsaturation levels of fatty acids and lipids, division of specific fatty acid species in the fatty acid pool and lipid pools, and lipid peroxidation level. Using two *Drosophila* PD models exhibiting mild or strong disease phenotypes, we demonstrated that α-syn neurotoxicity can be modulated by the lipid synthesis enzyme *mino*. RNAi against *mino* ameliorates α-syn-associated pathological phenotypes including the decline in locomotor activities and the loss of DA neurons, while elevated *mino* expression exacerbates these phenotypes. The beneficial effects of *mino* downregulation are similarly observed in α-syn flies harbouring RNAi species targeting the predicted differentially subcellular-localized *Gpat4*, and *CG15450*, suggesting a common

role of GPAT in modulating α-syn neurotoxicity. Notably, previous report indicated that fluorescence-tagged transgenic *mino*, when expressed in the female reproductive system, colocalized with both mitochondria and ER [65]. Although we detected mitochondrial localization of ectopically expressed α-syn in *Drosophila* photoreceptor neurons (data not shown), it is plausible that dynamic lipid exchange between mitochondria and ER contributes to the subcellular-independency of the modifier role of *GPAT* [66].

Our study also indicates that the modulation of higher-order oligomers of α-syn can potentially be achieved by employing RNAi targeting *GPAT*. The detection of α-syn oligomers in *Drosophila* brains through western blot has historically posed greater challenges compared to mammalian cells, despite successful identification of ectopically expressed α-syn in both TritonX-100 soluble and insoluble fractions [42,57,67]. Through an *in vivo* crosslinking with DTBP originally described by Cole and colleagues [58], we were able to enhance the sensitivity of detecting α-syn oligomeric species. While RNAi against *GPAT* did not result in a significant change in α-syn protein levels, we observed a relative redistribution of α-syn from higher-order oligomers to lower-order oligomers and monomers. This shift was associated with a decrease in α-syn neurotoxicity.

Interestingly, we observed a significantly accelerated mitochondria cumulative redox level in pan-neuronal α-syn-expressing fly brains during the first week, that preceded the onset of cell death from the second week onward. Although elevated α-syn is known to trigger caspase activation and apoptosis in various PD models [68,69], it remains uncertain if α-syn-induced neuronal death can occur through alternative pathways. Recent observations of enhanced lipid peroxidation in neurons containing *SNCA* gene triplication suggest their potential sensitivity to ferroptosis [26]. In the enzymatic ferroptotic pathway, lipoxygenase (LOX) catalyzes iron-dependent specific oxidation of poly-unsaturated PE-AA and PE-AdA [70]. Mitochondria, the primary ROS generating organelle, contributes to the non-enzymatic pathway of ferroptosis via Fenton reaction [71]. *Drosophila*, with a distinct lipidomic composition lacking polyunsaturated fatty acids including AA and AdA, may utilize shorter chain polyunsaturated fatty acids, such as linoleic acid (18:2n-6) and linolenic acid (18:3n-3), as substrates for ROS-induced non-enzymatic lipid peroxidation on ER and mitochondria [72,73]. Linoleic acid in choline glycerophospholipids is prone to form hydroperoxide during peroxidation in human erythrocytes membrane [74].The lipid peroxidation product 4-HNE has been observed in fat body, neurons, and muscles of aging flies and was further enhanced by paraquat feeding [75]. Although our results favor a model by which α-syn elicits neuronal death through ferroptosis, we cannot rule out apoptosis as a co-driver of neurodegeneration in this case. We appreciate that the TUNEL assay, which is commonly used for cell death detection, lacks specificity in distinguishing apoptosis, necrosis, and autolytic cell death [76], notwithstanding that TUNEL-positive nuclei have also been identified in cells undergoing ferroptosis [77]. Moreover, despite the absence of cleaved caspase 3 in our study, previous study using an hPARP-based apoptosis reporter has detected apoptosis in pan-neuronal α-syn-expressing brains in *Drosophila* [42]. It is therefore plausible that both apoptosis and ferroptosis coexist to drive neurodegeneration in α-syn fly brains [78].

Finally, we demonstrated in both the α-syn fly as well as primary mouse neuronal models that pharmacological inhibition of *mino*/GPAT activity through FSG67 treatment promotes beneficial outcomes that illustrates the transferability of our findings from non-mammalian to mammalian context. Notably, current disease-modifying experimental therapeutics for PD aimed at α-syn as a target are mostly focused on reducing its aggregation or enhancing its degradation. Our approach targeting a key pathway that α-syn acts on, i.e. lipid synthesis and modifications, offers a unique and at the same time complementary therapeutic angle that could augment the anti-aggregation, and/or pro-degradation approaches in mitigating α-syn-induced neurotoxicity. Interestingly, FSG67 was originally developed as a drug to treat obesity and diabetes [79]. Given the optimism surrounding the use of GLP agonists to treat PD, which was similarly first developed to treat diabetes (and subsequently to manage weight loss), it is interesting to postulate a converged pathway between FSG67 and GLP agonists that emphasizes the need to better understand the role of lipid aberrations in the pathogenesis of PD.

In conclusion, our research not only reveals a pivotal role of glycerol 3-phosphate acyltransferase in modulating α-syn aggregation and its neurotoxic effects, but also highlights its potential as a novel target for mitigating the progression of PD.

MATERIALS AND METHODS

Drosophila stocks

Flies were grown at 25°C with a standard yeast-corn meal-dextrose diet. Aging experiments were conducted at 25°C, unless otherwise stated. Adult male flies were gathered in groups of 20–30 per vial for aging. Throughout the aging process, the food was refreshed every two days for the initial two weeks and subsequently replaced daily from the third week onward. The *Drosophila* stocks used are listed in **Supplementary Table 1**.

Drosophila brain immunostaining

Larvae or adult fly brains were dissected in PBS, fixed in 3.7% paraformaldehyde in PBS with 0.1% Triton X-100 on ice for 0.5 hour, and subsequently fixed at room temperature for an additional 0.5 hour. Following fixation, brains were rinsed in PBS with 0.4% Triton X-100 (PBST) and subjected to primary antibodies staining for 1 day at 4°C, then washed in PBST and incubated in secondary antibodies for 1 day at 4°C, followed by washing with PBST. In the TUNEL assay, after removal of the buffer, the TUNEL reaction mixture was added, incubated in a 37°C water bath for 1h, and briefly washed. Subsequently, brains were stained in PBST with 4',6-diamidino-2-phenylindole (DAPI) for 3 hours, briefly washed, and mounted with Prolong Gold (Thermo Fisher Scientific) on bridged slides, positioned as a line with the anterior side facing upward and both sides padded with double layers of Scotch transparent tape (except for a single layer for TH staining in the PAM cluster). For cleaved caspase 3 staining, third instar larvae of w^{1118} or *hs-hid* were heat-shocked in a 37°C water bath for 2 hours and allowed to recover for 5 hours before dissection. Imaging was performed using an FV3000 confocal microscope with consistent image

settings for samples within each experiment. The primary antibodies used include rabbit anti-Tyrosine Hydroxylase TH (Pel Freeze, P40101-0, 1:500), rabbit anti-Cleaved Caspase-3 (Asp175) (Cell Signaling Technology, 9661, 1:500), rabbit anti-Cleaved Caspase-3 (Asp175) (5A1E) (Cell Signaling Technology, 9664, 1:500), mouse anti-Repo (DSHB, 8D12, 1:500), mouse anti-alpha-Tubulin (DSHB, 12G10, 1:5000), mouse anti-Malondialdehyde (Abcam, 11E3, ab243066, 1:500), mouse anti-4 Hydroxynonenal (Abcam, HNEJ-2, ab48506, 1:500), rabbit anti-α-syn (phospho S129) (Abcam, ab51253, 1:500).

Labkit-assisted Drosophila PAM cluster TH + neuron quantification

The TH + neurons within a single PAM cluster were imaged using FV3000 with 512x512 resolution and 0.34 µm slice interval for both TH and DAPI channels, generating z-stacks. Labkit training and TH + region prediction were performed on a computer featuring an NVIDIA Quadro P6000. Twenty representative z-stacks, encompassing a spectrum of TH signals and backgrounds, were vertically merged into a unified stack using Fiji/ImageJ. In Labkit (Fiji), the stack underwent more than 100 cycles of "scribbling-predicting-correcting" to train the TH + pixel classifier against backgrounds. The resulting classifier file with a size of 379 megabytes was applied consistently for subsequent TH + neuron analysis. For TH + region identification, the classifier file was loaded into Labkit to batch process a folder of z-stack TH images. The defects including noise and vacuoles on the Labkit-predicted mask images were further minimized using customized Matlab (Mathwork) code “Correct_Labkit_TH.m” (version 1.0, see the source code, instructions for installation and use, description of code dependencies and the test data in https://github.com/rmd13/FlyBrain_PAM_TH_DAPI_Labkit/). The code sequentially processes each slice of a Labkit-generated 0/1 mask image. It first smooths the mask using a Gaussian smoothing filter with a sigma of 1.5 to enhance the image quality. Following smoothing, a threshold of 0.25 is applied to the resulting image, thus only the pixels above this threshold are labeled as a new mask. This new mask slice is then dilated using a square-shaped structuring element with a width of 5 pixels. This step is crucial for filling in any small gaps or holes present within the TH + regions, ensuring that the mask is continuous. Additionally, the code identifies and addresses any larger holes that may still exist within the mask, provided these holes have an area of less than 200 pixels. These holes are filled to maintain the integrity of the mask. Finally, the mask is eroded using the same square-shaped structuring element with a width of 5 pixels. The above process helps to reduce the errors, resulting in a high-quality, refined mask suitable for subsequent image analysis steps. The processed mask images were imported into Imaris 8.4 (Bitplane) as a new channel alongside the raw images. TH + surfaces and DAPI spots were created using Imaris in the Labkit channel and DAPI channel, respectively. The number of TH + neurons in the PAM cluster was counted as DAPI spots located within the TH + surface by running the surface distance transformation extension (Imaris) outside the TH + surfaces.

Drosophila brain BODIPY C11 lipid peroxidation assay

Fly brains expressing pan-neuronal infrared fluorescent protein (mIFP) were dissected in PBS and transferred into in Eppendorf tube 1 containing 100 ul PBS. In Eppendorf tube 2, 0.5 ul of 5 mmol BODIPY C11 DMSO solution (Thermo Fisher Scientific, D3861) and 0.5 ul of 1% saponin (Sigma, S7900) were

added into 350 ul PBS (B), mixed and transferred to the tube 1, which was then rolled at room temperature for 30 min. Following the rolling process, brains were briefly washed in PBS and mounted with PBS on a bridged slide using two layers of Scotch transparent tape, creating a 5 mm gap. Thick nail polish was used to secure the four corners of the coverslip, and additional PBS was added to fill any gaps if necessary. BODIPY C11 was immediately imaged in FV3000 using a 100x objective lens. The brain optic lobe was located and live-imaged using a 640 nm laser to determine the position of labeled neuronal membranes. Subsequently, images were acquired in the green channel (488 nm laser, 0.04% laser power, 515–545 nm emission) and red channel (561 nm laser, 0.02% laser power, 575–605 nm emission), respectively. Five images were acquired for each brain. For each group the brains were imaged within 1 hour. The lipid peroxidation index was analyzed as the ratio of the mean intensity of membrane area in the green channel to the mean intensity in the red channel using ImageJ/Fiji. For each brain, the lipid peroxidation index from five images was averaged. A pseudo-colored image was generated by creating a ratio channel and masking out the unstained area in Imaris.

Drosophila daily locomotor activity assay

Fly food, extracted from a vial, was trimmed into two semi-circles with a height of 5 mm, and then positioned on 3 layers of 5 cm x 5 cm tissue paper with smooth side up for a 0.5 hour drying period. To administer FSG67 (HY-112489, MedChemExpress LLC), 10 µl of 0 mmol,1 mmol, 2.5 mmol, or 5 mmol FSG67 solution in PBS was introduced to the smooth side of fly food and evenly distributed until complete absorption. One end of clean glass tube for locomotor activity assay was inserted down vertically into the food and capped. Anesthetized enclosed flies were individually transferred into each tube, and then the tube was blocked with a sponge on the opposite side. These loaded glass tubes were then affixed to the DAM2 *Drosophila* activity monitors (TriKinetics). The locomotor activities were recorded at a frequency of 10 s over a period of one to three weeks, maintaining a 12-hour light/dark cycles of LED illumination controlled via an Arduino-controlled relay by the same computer. The food was replaced every three days. Actograms captured during this period were analyzed using the ActogramJ plugin [80] in ImageJ/Fiji. Daily locomotor activities were further analyzed and plotted using Excel 2010 and GraphPad Prism 6.01.

Western blot

Fly brains were dissected in PBS and homogenized with pestles in brain lysis buffer (Tris-HCl, pH 8.0 10 mmol, NaCl 200 mmol, Triton X-100 1%, EDTA 5 mmol, Glycerol 5%, PMSF 0.5 mmol, DTT 1 mmol, protease inhibitor cocktail (Roche, 11873580001)). Subsequently, an equal volume of 2X laemmli loading buffer (Tris-HCl, pH 6.8, 125 mmol, bromophenol blue 0.02%, SDS 4%, glycerol 20%, β-mercaptoethanol 10%) was added and heated at 50^{o}C for 0.5 hour. For detection of α-syn oligomers, fly brains were dissected in PBS and cross-linked in same-day prepared buffer A (HEPES 20 mmol pH 8.5, KCl 120 mmol, EDTA 2 mmol, sucrose 0.25 M, glycerol 1%, Dimethyl dithiobispropionimidate (DTBP) 4 mmol, protease inhibitor cocktail (Roche)) on ice for 1h. Then reaction was halted by adding 10 mmol Tris-HCl pH 8.8 for

10 min on ice. Brains were homogenized with a pestle, and an equal volume of 2X Laemmli loading buffer was added without β-mercaptoethanol or DTT, followed by heating at 50^{o}C for 0.5 hour. The samples were loaded into Mini Protean TGX (stain-free) 4–20% gel (Bio-Rad, 4568095) to run for 100V 1.5 hour. The gel was UV-activated and transferred onto PVDF membrane using transfer buffer (Tris 25 mmol, Glycine 192 mmol, 20% methanol) at 100V for 1.5 hour. The membrane was fixed in PBS with 3.7% PFA and 0.025% glutaraldehyde for 0.5 hour, stain-free imaged, and blocked in 5% milk in Tris-buffered saline with 0.1% Tween-20 (TBST). Primary antibodies used include mouse anti-α-syn (BD 610787, 1:1000), rabbit anti-Gpi (Merck, HPA024305, 1:1000), rabbit anti-LDH (Thermo Fisher,PA5-26531, 1:1000), and secondary antibodies include anti-mouse HRP (CST, 7076S, 1:3000) and anti-rabbit HRP (Amersham, NA934-1ML, 1:3000). The HRP was detected using WesternBright Sirius in ChemiDoc (Bio-rad). The membrane was subsequently re-blotted with mouse anti-alpha tubulin (DSHB, 12G10, 1:5000). Image was analyzed using Image Lab (Bio-Rad) and ImageJ/Fiji, and the results were plotted in GraphPad prism.

Mito-roGFP2-Orp1 imaging for H_2O_2

Retina expressing mito-roGFP2-Orp1 were dissected in PBS and fixed in PBS with 3.7% PFA, 0.1% Triton X-100 and 20 mmol N-Ethylmaleimide (Thermo Fisher Scientific, 23030) for 0.5 hour on ice, followed by another 0.5 hour at room temperature. The fixed retina was washed in PBST with 5% goat serum overnight at 4^{o}C and then was mounted with Prolong Gold anti-fade mountant (Thermo Fisher Scientific, P10144). Mito-roGFP2-Orp1 was imaged by exciting with a 405 nm or 488 nm laser, respectively, and collecting 500–530 nm emission light. The H_2O_2 index was determined by the ratio of mean intensity of the mitochondria in the two channels using ImageJ/Fiji.

MitoTimer imaging for cumulative redox history

Brains were dissected in PBS and fixed in PBS with 3.7% PFA and 0.1% Triton X-100 for 0.5 hour on ice and an additional 0.5 hour at room temperature. Following fixation, the brains were washed in PBST with 5% goat serum and DAPI overnight at 4^{o}C and then mounted with Prolong Gold anti-fade mountant (Thermo Fisher Scientific, P10144). The green channel (488 nm laser, 500–540 nm emission) and the red channel (561 nm laser, 570–620 nm emission) were imaged on the cortex layer of the optic lobe. The ratio of the mean intensity of MitoTimer between the red and the green channel was analyzed using ImageJ/Fiji.

Drosophila climbing assay and quantification

The climbing assay was conducted on a customized workstation composed of a background white foam, side LED light, bottom light, 50 ml glass cylinders, an elastic cushion, and a Nikon digital camera securely affixed to a tripod. A sponge pad was positioned in the inner bottom of the cylinder to minimize potential harm to the flies during the climbing assay. 10 ~ 20 flies were flipped into a capped cylinder, tapped to the

bottom and allowed to climb for 5 s, following which an image was promptly captured using the camera. The average climbing height for all the images was analyzed using a customized FlySpotter program (Srinivas Gorur-Shandilya, https://github.com/sg-s/fly-spotter) and graphically represented using GraphPad prism.

Real-time PCR for quantitative of fly brain transcripts

Fly brains of 3-weeks old were dissected in PBS, with trachea sacs and fat bodies detached, were subsequently transferred into RNAlater (Thermo Fisher Scientific, R0901). Following removal of excess fluid, RNA from the brain was extracted using TRIzol™ Reagent (Thermo Fisher Scientific, 15596026). The extracted RNA was treated with dsDNase (Thermo Fisher Scientific, EN0771). Subsequently, cDNA was prepared using Invitrogen SuperScripII First-Strand Synthesis System for RT-PCR (11904-018). qPCR was performed using iQ™ SYBR Green Supermix (Bio-rad, 1708882) and LightCycler 96 Instrument (Roche). The data was analyzed using LightCycler 96 software (Roche). RPL32 served as an internal control for mRNA quantification. The qPCR primers used include mino-F1: CAAGCCATCTGCCAGGGTCC, mino-R1: GACATCACAGAGGTGGCTGCTG, RpL32-qF1: ATGCTAAGCTGTCGCACAAATG, RpL32-qR1: GCTTGTTCGATCCGTAACCG.

Synuclein Preformed fibrils preparation

15µl of 2mg/ml synuclein PFF (StressMarq SPR-324) aliquoted into screw-capped tubes were sonicated in an ultrasonic bath sonicator for 2.5h at the following conditions: Sweep, 37Hz frequency, 60% power. Water was changed at 30mins interval to maintain the water temperature at 15°C.

Mouse primary neuron culture and staining

Mice-related studies were approved by and conformed to the guidelines of the Institutional Animal Care Committee (IACUC) of the Nanyang Technological University Lee Kong Chian School of Medicine. Embryonic day 17.5 mouse fetuses from C57BL/6 were obtained. The cortices were isolated and dissociated with papain (LS003119, Worthington) for 30 min at 37°C. Papain was removed and cortices were washed with DMEM/FBS and spin down at 1,000rpm, 5 mins. Cells were titrated, spin down and resuspended in Neurobasal medium supplemented with B27 and GlutaMAX (Gibco). 80,000 cells/ well were plated. At day 7, mice primary cortical neurons were treated with 1µg/ml α-syn monomers (SPR-323, StressMarq) or 1µg/ml synuclein PFF (SPR-322, StressMarq) with or without 75 mmol FSG (HY-112489, MedChemExpress LLC) for 2 weeks. Following treatment, cells were fixed in 4% PFA/4% sucrose/PBS for 30 minutes at room temperature, then washed three times with PBS. Subsequently, cells were blocked in 0.2 M glycine, 0.1 mg/ml saponin, and 30 mg/ml BSA in PBS for 45 minutes. Primary antibodies staining was carried out in antibody diluent (0.1 mg/ml saponin and 1 mg/ml BSA in PBS) for 1 hour at room temperature using anti-Malondialdehyde antibody (Abcam, 11E3, ab243066, 1:500), anti-4-Hydroxynonenal antibody (Abcam, HNEJ-2, ab48506, 1:500) and anti-α-syn phospho S129 (Abcam, ab51253, 1:500). After washing three times with PBS, cells were incubated with secondary antibodies in

antibody diluent for 1 hour, followed by four washes with PBS. Finally, cells were stained with BODIPY 493/503 (Thermo Fisher Scientific, D-3922, 1:1000) and 1 μg/ml DAPI, mounted, and imaged using an FV3000 confocal microscope (Olympus). For lipid peroxidation assay, 5 mmol BODIPY C11 was added to the culture medium of glass-bottom culture dish in 1:1000 dilutions and incubated for 0.5 hour, then directly imaged in the green and red channel respectively. The ratio of mean intensity in the cell was analyzed using ImageJ/Fiji.

Statistics

Statistical analyses were conducted using Prism 8 (GraphPad) and Matlab (MathWorks). For the genetic screening, the Anderson-Darling test was applied to assess the non-normal distribution of all the data, followed by the Mann-Whitney U-test. The p-values were adjusted by the Benjamini-Hochberg method using the Matlab function padj = PVAL ADJUST (p-values, 'BH'), where p is the input vector of all the p-values (fakenmc/pval_adjust, version 1.2.0.2, by Nuno Fachada. https://github.com/nunofachada/pval_adjust). One-way or two-way ANOVA, supplemented by Tukey's and Dunnett's post hoc test, was used for multi-group comparisons. All tests were two-tailed. Sample sizes are specified in the figure legends. Data are presented as mean ± S.D. Significance levels are *$p < 0.05$, **$p < 0.01$, ***$p < 0.001$, and ****$p < 0.0001$.

Declarations

Data Availability

All the data is included in this manuscript and supplementary data.

Code Availability

The Labkit classifier file for PAM cluster neuron prediction and the code for the correction of Labkit-predicted TH+ regions could be downloaded from Github (https://github.com/rmd13/FlyBrain_PAM_TH_DAPI_Labkit). The code was under MIT license.

ACKNOWLEDGEMENTS

This work was supported by Singapore Ministry of Health Open Fund-Large Collaborative Grant (MOH-OFLCG000207) to K.L.L.

AUTHOR CONTRIBUTIONS

M.R. and K.L.L. participated in the design of experiments, data analysis, and interpretation. W.T and G.G.Y.L. designed and performed the experiments using primary mouse neurons. M.R. and K.L. wrote the manuscript with inputs from all the authors.

CONFLICT OF INTERESTS

The authors declare no competing interests.

References

1. Kalia, L. V. & Lang, A. E. Parkinson's disease. *The Lancet* **386**, 896-912 (2015).
2. Kim, H. J. Alpha-synuclein expression in patients with Parkinson's disease: a clinician's perspective. *Exp Neurobiol* **22**, 77-83 (2013).
3. Puschmann, A. et al. Alpha-synuclein multiplications with parkinsonism, dementia or progressive myoclonus? *Parkinsonism Relat Disord* **15**, 390-392 (2009).
4. Krüger, R. et al. Ala30Pro mutation in the gene encoding alpha-synuclein in Parkinson's disease. *Nat Genet* **18**, 106-108 (1998).
5. Polymeropoulos, M. H. et al. Mutation in the alpha-synuclein gene identified in families with Parkinson's disease. *Science* **276**, 2045-2047 (1997).
6. Nalls, M. A. et al. Identification of novel risk loci, causal insights, and heritable risk for Parkinson's disease: a meta-analysis of genome-wide association studies. *Lancet Neurol* **18**, 1091-1102 (2019).
7. Zhang, Y. et al. A comprehensive analysis of the association between SNCA polymorphisms and the risk of Parkinson's disease. *Front Mol Neurosci* **11**, 391 (2018).
8. Zuk, O., Hechter, E., Sunyaev, S. R. & Lander, E. S. The mystery of missing heritability: genetic interactions create phantom heritability. *Proc Natl Acad Sci USA* **109**, 1193-1198 (2012).
9. Mullin, S. & Schapira, A. The genetics of Parkinson's disease. *British Medical Bulletin* **114**, 39-52 (2015).
10. Lee, R. M. Q. & Koh, T.-W. Genetic modifiers of synucleinopathies—lessons from experimental models. *Oxford Open Neuroscience* **2**, 1-30 (2023).
11. Moors, T. E. et al. The subcellular arrangement of alpha-synuclein proteoforms in the Parkinson's disease brain as revealed by multicolor STED microscopy. *Acta Neuropathol* **142**, 423-448 (2021).
12. Shahmoradian, S. H. et al. Lewy pathology in Parkinson’s disease consists of crowded organelles and lipid membranes. *Nature Neuroscience* **22**, 1099-1109 (2019).
13. Fais, M. et al. Parkinson's disease-related genes and lipid alteration. *Int J Mol Sci* **22**, 7630 (2021).
14. Galper, J. et al. Lipid pathway dysfunction is prevalent in patients with Parkinson's disease. *Brain* **0**, 1-16 (2022).
15. Sun, W.-Y. et al. Phospholipase iPLA2β averts ferroptosis by eliminating a redox lipid death signal. *Nature Chemical Biology* **17**, 465–476 (2021).
16. Chiurchiù, V. et al. Lipidomics of bioactive lipids in Alzheimer's and Parkinson's diseases: where are we? *Int J Mol Sci* **23**, 6235 (2022).
17. Avisar, H. et al. Lipid level alteration in human and cellular models of alpha synuclein mutations. *NPJ Parkinson's disease* **8**, 52 (2022).

18. Alecu, I. & Bennett, S. A. L. Dysregulated lipid metabolism and its role in α-synucleinopathy in Parkinson's disease. *Frontiers in Neuroscience* **13**, 328 (2019).
19. Mori, A., Imai, Y. & Hattori, N. Lipids: key players that modulate α-synuclein toxicity and neurodegeneration in Parkinson's disease. *International Journal of Molecular Sciences* **21**, 3301 (2020).
20. Jo, E., Fuller, N., Rand, R. P., St George-Hyslop, P. & Fraser, P. E. Defective membrane interactions of familial Parkinson's disease mutant A30P alpha-synuclein. *J Mol Biol* **315**, 799-807 (2002).
21. Tripathi, A. et al. Pathogenic mechanisms of cytosolic and membrane-enriched α-synuclein converge on fatty acid homeostasis. *The Journal of Neuroscience* **42**, 2116-2130 (2022).
22. Barceló-Coblijn, G., Golovko, M. Y., Weinhofer, I., Berger, J. & Murphy, E. J. Brain neutral lipids mass is increased in alpha-synuclein gene-ablated mice. *J Neurochem* **101**, 132-141 (2007).
23. Golovko, M. Y., Rosenberger, T. A., Feddersen, S., Faergeman, N. J. & Murphy, E. J. Alpha-synuclein gene ablation increases docosahexaenoic acid incorporation and turnover in brain phospholipids. *J Neurochem* **101**, 201-211 (2007).
24. Golovko, M. Y. et al. α-Synuclein Gene Deletion Decreases Brain Palmitate Uptake and Alters the Palmitate Metabolism in the Absence of α-Synuclein Palmitate Binding. *Biochemistry* **44**, 8251-8259 (2005).
25. Outeiro, T. F. & Lindquist, S. Yeast cells provide insight into alpha-synuclein biology and pathobiology. *Science* **302**, 1772-1775 (2003).
26. Mahoney-Sanchez, L. et al. Alpha synuclein determines ferroptosis sensitivity in dopaminergic neurons via modulation of ether-phospholipid membrane composition. *Cell Reports* **40**, 111231 (2022).
27. Angelova, P. R. et al. Alpha synuclein aggregation drives ferroptosis: an interplay of iron, calcium and lipid peroxidation. *Cell Death & Differentiation* **10**, 2781-2796 (2020).
28. Imberdis, T. et al. Cell models of lipid-rich α-synuclein aggregation validate known modifiers of α-synuclein biology and identify stearoyl-CoA desaturase. *Proc Natl Acad Sci U S A* **116**, 20760-20769 (2019).
29. Nuber, S. et al. A brain-penetrant stearoyl-CoA desaturase inhibitor reverses α-synuclein toxicity. *Neurotherapeutics* **19**, 1018-1036 (2022).
30. Nuber, S. et al. A stearoyl-Coenzyme A desaturase inhibitor prevents multiple Parkinson disease phenotypes in α-synuclein mice. *Ann Neurol* **89**, 74-90 (2021).
31. Terry-Kantor, E. et al. Rapid alpha-synuclein toxicity in a neural cell model and its rescue by a stearoyl-CoA desaturase inhibitor. *Int J Mol Sci* **21**, 5193 (2020).
32. Vincent, B. M. et al. Inhibiting stearoyl-CoA desaturase ameliorates α-synuclein cytotoxicity. *Cell Rep* **25**, 2742-2754 (2018).
33. Golovko, M. Y. et al. Acyl-CoA synthetase activity links wild-type but not mutant alpha-synuclein to brain arachidonate metabolism. *Biochemistry* **45**, 6956-6966 (2006).

34. Zou, Y. et al. A GPX4-dependent cancer cell state underlies the clear-cell morphology and confers sensitivity to ferroptosis. *Nat Commun* **10**, 1617 (2019).
35. Nicholatos, J. W., Tran, D., Liu, Y., Hirst, W. D. & Weihofen, A. Lysophosphatidylcholine acyltransferase 1 promotes pathology and toxicity in two distinct cell-based alpha-synuclein models. *Neurosci Lett* **772**, 136491 (2022).
36. Fanning, S. et al. Lipase regulation of cellular fatty acid homeostasis as a Parkinson's disease therapeutic strategy. *NPJ Parkinson's disease* **8**, 74 (2022).
37. Jansen, I. E. et al. Discovery and functional prioritization of Parkinson's disease candidate genes from large-scale whole exome sequencing. *Genome Biol* **18**, 22 (2017).
38. Yan, J. et al. Systematic analysis of binding of transcription factors to noncoding variants. *Nature* **591**, 147-151 (2021).
39. Grenn, F. P. et al. The Parkinson's disease genome-wide association study locus browser. *Movement Disorders* **35**, 2056-2067 (2020).
40. Hu, Y. et al. An integrative approach to ortholog prediction for disease-focused and other functional studies. *BMC Bioinformatics* **12**, 357 (2011).
41. Ren, M. et al. MED13 and glycolysis are conserved modifiers of α-synuclein-associated neurodegeneration. *Cell Reports* **41**, 111852 (2022).
42. Ordonez, D. G., Lee, M. K. & Feany, M. B. Alpha-synuclein induces mitochondrial dysfunction through spectrin and the actin cytoskeleton. *Neuron* **97**, 108-124 (2018).
43. Sun, J. et al. Neural control of startle-induced locomotion by the mushroom bodies and associated neurons in Drosophila. *Frontiers in Systems Neuroscience* **12** (2018).
44. Riemensperger, T. et al. A single dopamine pathway underlies progressive locomotor deficits in a Drosophila model of Parkinson disease. *Cell reports* **5**, 952-960 (2013).
45. Arzt, M. et al. Labkit: Labeling and segmentation toolkit for big image data. *Frontiers in Computer Science* **4** (2022).
46. Valadas, J. S. et al. Er lipid defects in neuropeptidergic neurons impair sleep patterns in Parkinson’s disease. *Neuron* **98**, 1155-1169 (2018).
47. Cuvelier, E. et al. Overexpression of wild-type human alpha-synuclein causes metabolism abnormalities in Thy1-asyn transgenic mice. *Frontiers in Molecular Neuroscience* **11** (2018).
48. Gajula Balija, M. B., Griesinger, C., Herzig, A., Zweckstetter, M. & Jackle, H. Pre-fibrillar alpha-synuclein mutants cause Parkinson's disease-like non-motor symptoms in Drosophila. *PLoS One* **6**, e24701 (2011).
49. Angelova, P. R. et al. Lipid peroxidation is essential for α-synuclein-induced cell death. *J Neurochem* **133**, 582-589 (2015).
50. Mahoney-Sánchez, L. et al. Ferroptosis and its potential role in the physiopathology of Parkinson’s disease. *Progress in Neurobiology* **196**, 101890 (2021).

51. Yu, D. et al. A naturally monomeric infrared fluorescent protein for protein labeling in vivo. *Nature methods* **12**, 763-765 (2015).
52. Takeuchi, K. & Reue, K. Biochemistry, physiology, and genetics of GPAT, AGPAT, and lipin enzymes in triglyceride synthesis. *Am J Physiol Endocrinol Metab* **296**, E1195-1209 (2009).
53. Jiang, Y. et al. MULocDeep: A deep-learning framework for protein subcellular and suborganellar localization prediction with residue-level interpretation. *Comput Struct Biotechnol J* **19**, 4825-4839 (2021).
54. Kuhajda, F. P. et al. Pharmacological glycerol-3-phosphate acyltransferase inhibition decreases food intake and adiposity and increases insulin sensitivity in diet-induced obesity. *Am J Physiol Regul Integr Comp Physiol* **301**, 116-130 (2011).
55. Choi, M. L. et al. Pathological structural conversion of α-synuclein at the mitochondria induces neuronal toxicity. *Nature Neuroscience* **25**, 1134-1148 (2022).
56. Dada, S. T. et al. Spontaneous nucleation and fast aggregate-dependent proliferation of α-synuclein aggregates within liquid condensates at neutral pH. *Proc Natl Acad Sci U S A* **120**, e2208792120 (2023).
57. Olsen, A. L., Clemens, S. G. & Feany, M. B. Nicotine-mediated rescue of α-synuclein toxicity requires synaptic vesicle glycoprotein 2 in Drosophila. *Movement disorders : official journal of the Movement Disorder Society* **38**, 244-255 (2023).
58. Cole, N. B. et al. Lipid droplet binding and oligomerization properties of the Parkinson's disease protein alpha-synuclein. *J Biol Chem* **277**, 6344-6352 (2002).
59. Albrecht, S. C., Barata, A. G., Grosshans, J., Teleman, A. a. & Dick, T. P. In vivo mapping of hydrogen peroxide and oxidized glutathione reveals chemical and regional specificity of redox homeostasis. *Cell metabolism* **14**, 819-829 (2011).
60. Laker, R. C. et al. A novel mitotimer reporter gene for mitochondrial content, structure, stress, and damage in vivo. *Journal of Biological Chemistry* **289**, 12005-12015 (2014).
61. Jo, E., McLaurin, J., Yip, C. M., St. George-Hyslop, P. & Fraser, P. E. A-synuclein membrane interactions and lipid specificity. *Journal of Biological Chemistry* **275**, 34328-34334 (2000).
62. Kiechle, M., Grozdanov, V. & Danzer, K. M. The role of lipids in the initiation of α-synuclein misfolding. *Frontiers in Cell and Developmental Biology* **8** (2020).
63. Middleton, E. R. & Rhoades, E. Effects of curvature and composition on α-synuclein binding to lipid vesicles. *Biophys J* **99**, 2279-2788 (2010).
64. Galvagnion, C. et al. Lipid vesicles trigger α-synuclein aggregation by stimulating primary nucleation. *Nat Chem Biol* **11**, 229-234 (2015).
65. Vagin, V. V. et al. Minotaur is critical for primary piRNA biogenesis. *Rna* **19**, 1064-1077 (2013).
66. Tatsuta, T., Scharwey, M. & Langer, T. Mitochondrial lipid trafficking. *Trends in Cell Biology* **24**, 44-52 (2014).

67. Gu, X.-L. et al. Astrocytic expression of Parkinson's disease-related A53T -synuclein causes neurodegeneration in mice. *Molecular brain* **3**, 12 (2010).
68. Cookson, M. R. α-Synuclein and neuronal cell death. *Molecular Neurodegeneration* **4**, 9 (2009).
69. Yamada, M., Iwatsubo, T., Mizuno, Y. & Mochizuki, H. Overexpression of alpha-synuclein in rat substantia nigra results in loss of dopaminergic neurons, phosphorylation of alpha-synuclein and activation of caspase-9: resemblance to pathogenetic changes in Parkinson's disease. *J Neurochem* **91**, 451-461 (2004).
70. Bayır, H. et al. Achieving life through death: Redox biology of lipid peroxidation in ferroptosis. *Cell Chem Biol* **27**, 387-408 (2020).
71. Lin, K.-J. et al. Iron brain menace: The involvement of ferroptosis in Parkinson disease. *Cells* **11**, 3829 (2022).
72. Shen, L. R. et al. Drosophila lacks C20 and C22 PUFAs. *J Lipid Res* **51**, 2985-2992 (2010).
73. Yoshioka, T. et al. Evidence that arachidonic acid is deficient in phosphatidylinositol of Drosophila heads. *J Biochem* **98**, 657-662 (1985).
74. Guo, L., Ogamo, A., Ou, Z., Shinozuka, T. & Nakagawa, Y. Preferential formation of the hydroperoxide of linoleic acid in choline glycerophospholipids in human erythrocytes membrane during peroxidation with an azo initiator. *Free Radic Biol Med* **18**, 1003-1012 (1995).
75. Zheng, J., Mutcherson, R., II & Helfand, S. L. Calorie restriction delays lipid oxidative damage in Drosophila melanogaster. *Aging Cell* **4**, 209-216 (2005).
76. Grasl-Kraupp, B. et al. In situ detection of fragmented DNA (TUNEL assay) fails to discriminate among apoptosis, necrosis, and autolytic cell death: a cautionary note. *Hepatology* **21**, 1465-1468 (1995).
77. He, Z. et al. Role of ferroptosis induced by a high concentration of calcium oxalate in the formation and development of urolithiasis. *Int J Mol Med* **47**, 289-301 (2021).
78. Su, L.-J. et al. Reactive oxygen species-induced lipid peroxidation in apoptosis, autophagy, and ferroptosis. *Oxidative Medicine and Cellular Longevity* **2019**, 5080843 (2019).
79. Wydysh, E. A., Medghalchi, S. M., Vadlamudi, A. & Townsend, C. A. Design and synthesis of small molecule glycerol 3-phosphate acyltransferase inhibitors. *J Med Chem* **52**, 3317-3327 (2009).
80. Schmid, B., Helfrich-Förster, C. & Yoshii, T. A new imagej plug-in “ActogramJ” for chronobiological analyses. *Journal of Biological Rhythms* **26**, 464-467 (2011).

Figures

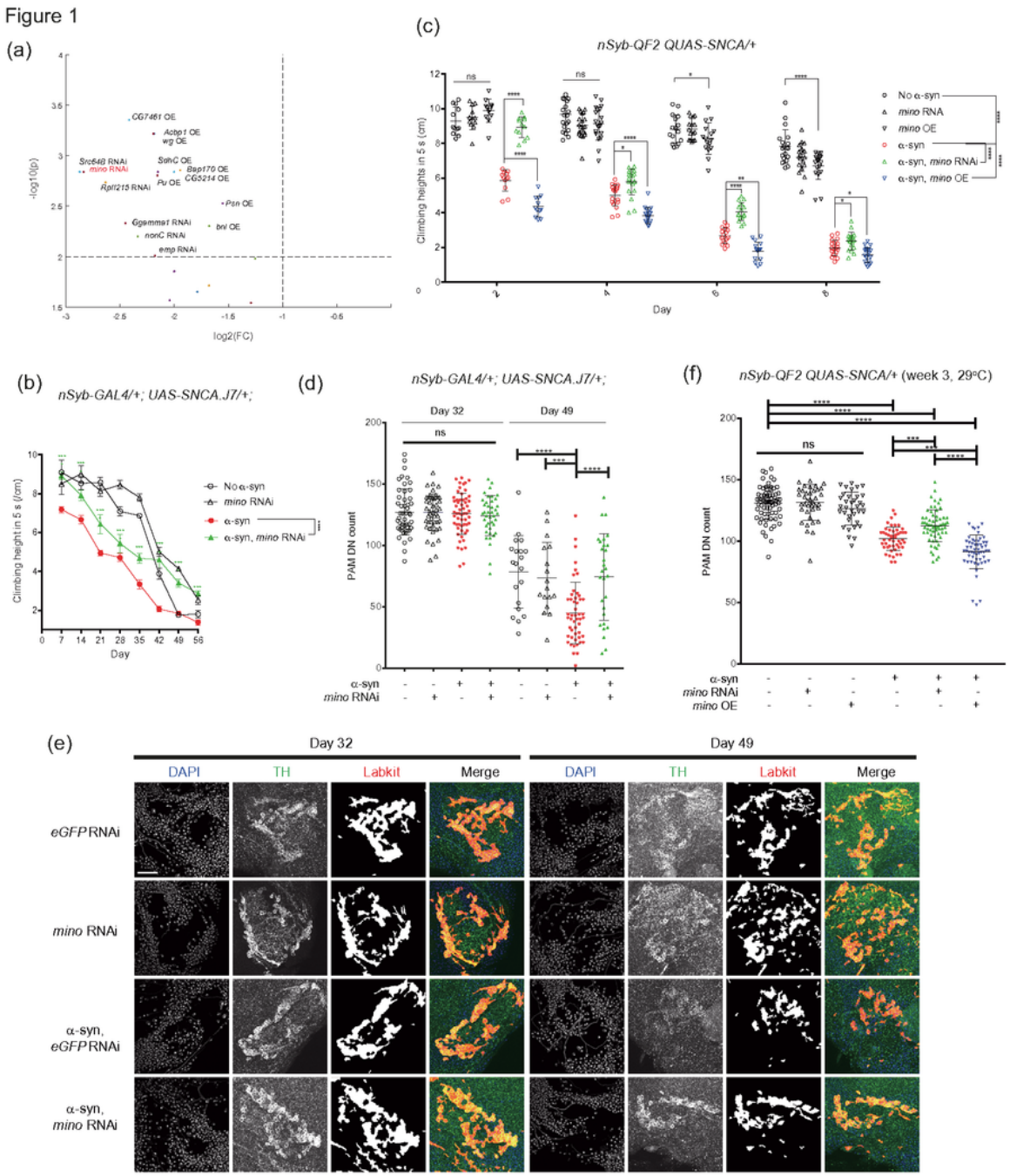

Figure 1

***Drosophila* genetic screen identifies *mino*RNAi as a suppressor of a-syn neurotoxicity.** (**a**) Plot of fold change (FC) of the size of a-syn-induced lamina vacuoles vs. BH-adjusted p-value of Mann-Whitney U test of genetic screen for a-syn modifiers using *eGFP* RNAi as control. The genes with RNAi or overexpression (OE) having FC > 2 and p < 0.01 were labeled. Each data point was generate by Matlab function plot(log2(FC), −log10(p-value),'.') using FC and p-value for one group. (**b**, **c**) *mino* knockdown suppressed

the a-syn-induced decline of startle-induced climbing ability in two independent synucleinopathy models of pan-neuronal a-syn-expressing flies with genotypes *nSyb-GAL4/+; UAS-SNCA.J7/+* (**b**) and *nSyb-QF2 QUAS-SNCA/+* (**c**). *mino* overexpression further exacerbated the a-syn-induced decline of climbing height (**c**). Each data point indicated the mean climbing height of one vial of 20 flies. The total number of vials for each group (*N*) is between 12 and 25. Measurements were taken from distinct samples for each timepoint, and were measured repeatedly across timepoints. (**d**, **e**, **f**) *mino*knockdown suppressed the a-syn-induced loss of dopaminergic neurons (DN) in the PAM cluster in two independent synucleinopathy models of pan-neuronal a-syn-expressing flies (*nSyb-GAL4/+; UAS-SNCA.J7/+*) (**d**, **e**) and (*nSyb-QF2 QUAS-SNCA/+*) (**f**). *mino* overexpression exacerbated the a-syn-induced loss of DN (**f**). TH+ neurons were trained and identified semi-automatically using Labkit and then quantified by DAPI spots that were located inside the TH-positive neurons (**e**). Measurements were taken from distinct samples. *N* = 50, 48, 57, 40, 20, 17, 50, 29 for (**d**), and 71, 39, 35, 50, 64, 55 for (**f**), from left to right. Scale bar represents 20 mm for (**e**). Data in (**b**, **c**, **d**, **f**) at each timepoint were analyzed with one-way ANOVA followed by Tukey's and Dunnett's multiple comparisons test. The group effects in (**b**) and (**c**) were analyzed using two-way ANOVA followed by Tukey's and Dunnett's multiple comparisons test. Each data point indicates one biological replicate from the mean climbing height of 1 vial of 20~30 flies in (**b**) and (**c**), and from one brain in (**d**) and (**f**). Data are presented as mean ± S.D. *p < 0.05, **p < 0.01, ***p < 0.001, and ****p < 0.0001.

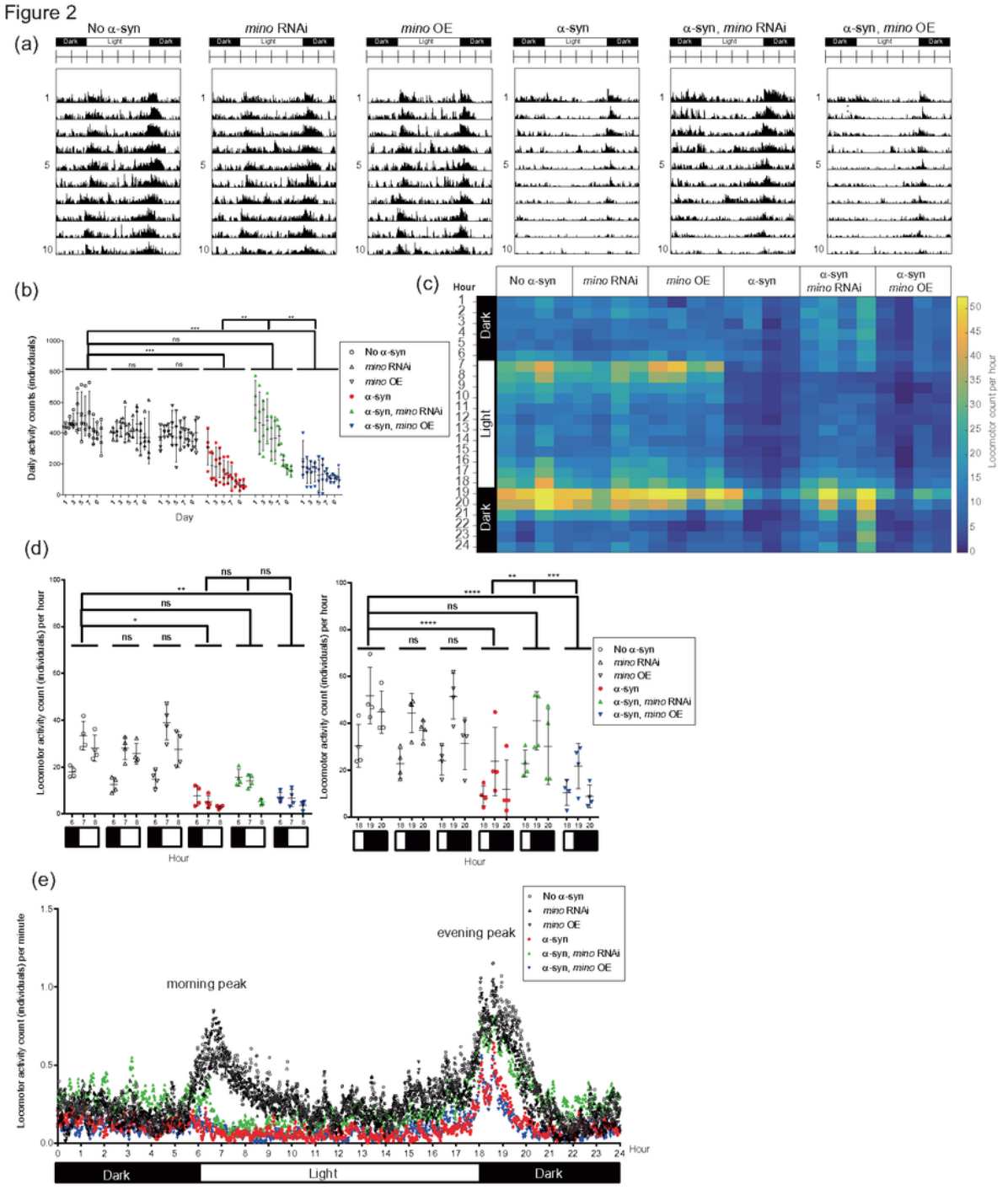

Figure 2

***mino* RNAi suppresses the a-syn-induced decline of daily locomotor activity.** (**a**, **b**) Mean actograms (**a**) and quantification of daily locomotor activities (**b**) recorded using *Drosophila*activities monitor (DAM) for flies with or without pan-neuronal a-syn (*nSyb-QF2 QUAS-SNCA/+*) and/or *mino*RNAi or overexpression. *mino* RNAi suppressed the a-syn-induced decline of daily total locomotor activities recorded from day 1 onwards. (**c**, **d**, **e**) *mino* RNAi enhanced the circadian-related locomotor activity in the light/dark transition.

Heatmap of average hourly locomotor activities for individual flies (**c**). *mino*RNAi affects the hourly locomotor activities around the light/dark transition (7 hours to 10 hours), but not the dark/light transition (1 hour to 4 hours) (**d**). Distribution of mean locomotor activities per minute (**e**). Measurements were taken from distinct samples for each timepoint, and were measured repeatedly across timepoints. *N* = 40. Data in (**b**, **d**) were analyzed with two-way ANOVA followed by Tukey's and Dunnett's multiple comparisons test. Each data point for one timepoint indicates one biological replicate. Data are presented as mean ± S.D. *p < 0.05, **p < 0.01, ***p < 0.001, and ****p < 0.0001.

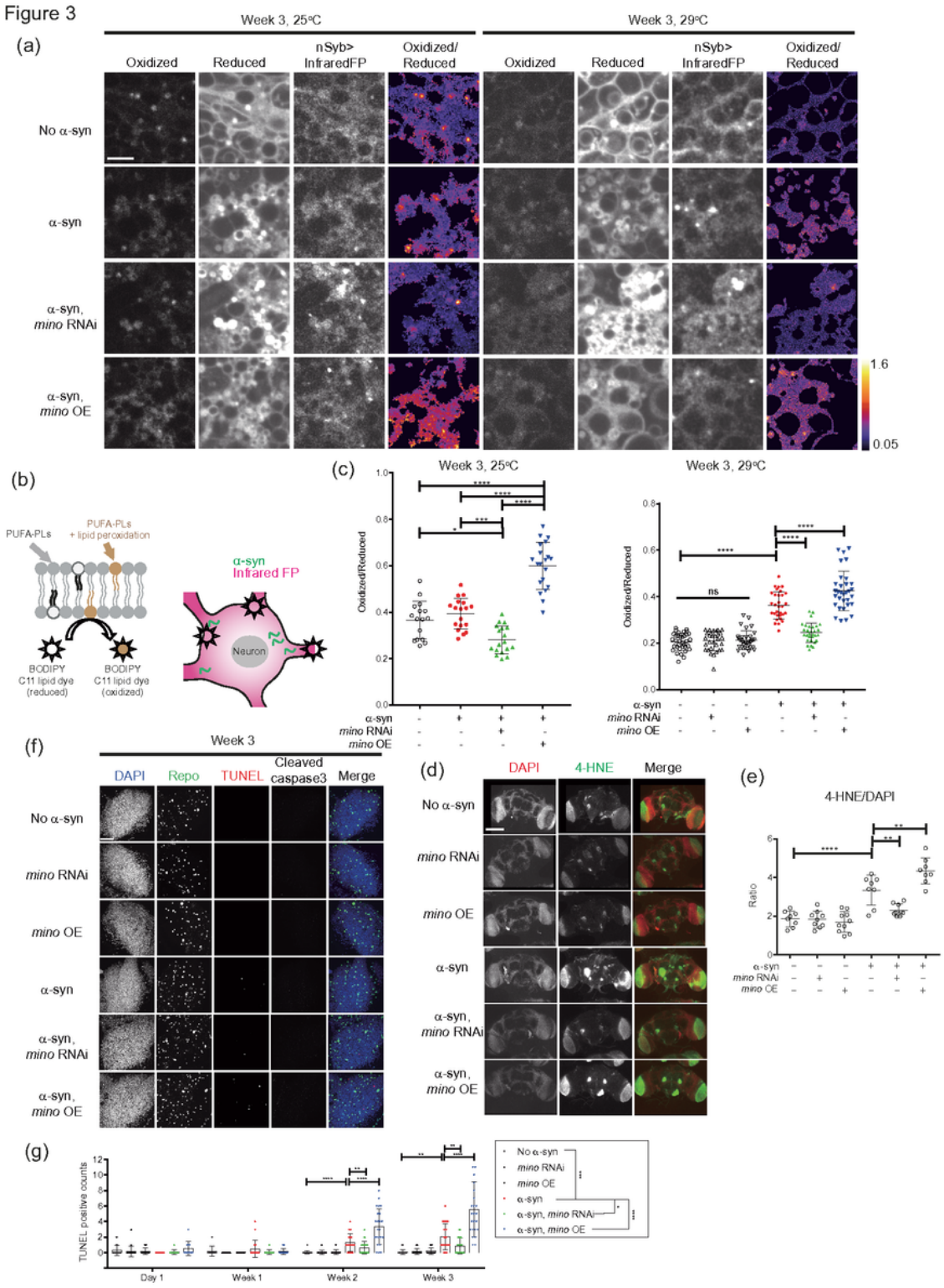

Figure 3

***mino* modulates a-syn-induced lipid peroxidation on neuronal lipid membranes and caspase-3-independent cell death.** (**a**) *mino* regulated neuronal membrane lipid peroxidation levels in an a-syn-dependent manner. BODIPY C11 staining for lipid peroxidation in the optic lobes of flies incubated at 25^{o}C or 29^{o}C for 3 weeks. Oxidized and reduced C11 were imaged using 488 nm laser and 546 nm laser, respectively. The neuronal membrane was located by pan-neuronal expression of mIFP. The pixel ratio between oxidized C11 and reduced C11 in the mIFP-labeled membrane region was shown as pseudo-colouring heatmap. (**b**) Schematic illustration of BODIPY C11 staining and neuronal membrane labeling in fly brains. Neuronal membranes were labeled by pan-neuronal infrared fluorescent proteins (*nSyb-GAL4/UAS-CD4-mIFP-T2A-HO1*). The PUFA-containing membrane lipid that undergoes lipid oxidation could further oxidize the C11 dye and change its emission spectrum. (**c**) Quantification of the mean ratio of oxidized to reduced C11 in the optic lobes of flies incubated at 25^{o}C or 29^{o}C for 3 weeks. Each data point indicated the average lipid peroxidation level of one fly, averaged from 4 images. *N* = 16, 18, 18, 20; 35, 30, 33, 31, 30, 32, from left to right. (**d**) Staining for DAPI and the lipid peroxidation product 4-HNE in the optic lobes of flies incubated at 29^{o}C for 3 weeks. Maximum intensity projection (MIP) of z-sack was shown. (**e**) Quantification of mean intensity of MIP for 4-HNE normalized to DAPI in the optic lobes. *N* = 8, 9, 10, 8, 9, 8, from left to right. Measurements were taken from distinct samples for each timepoint and also across timepoints. (**f**) Staining for DAPI, Repo, TUNEL, and cleaved caspase-3 in optic lobes of flies incubated at 29^{o}C for 3 weeks. (**g**) Quantification of TUNEL-positive DAPI-labeled nuclei per optic lobe of one fly for 1 day, 1 week, 2 weeks and 3 weeks. *N* = 24, 22, 20, 10, 10, 11; 10, 12, 11, 20, 22, 23; 22, 26, 21, 24, 26, 23; 24, 25, 23, 26, 27, 24, from left to right. Scale bars represent 3 mm for (**a**), 150 mm for (**d**) and 30 mm for (**f**). Data in (**c**, **e**, **g**) were analyzed with one-way ANOVA followed by Tukey's and Dunnett's multiple comparisons test, or non-parametric unpaired t-Test (**g**). The group effects in (**g**) were analyzed using two-way ANOVA followed by Tukey's and Dunnett's multiple comparisons test. Each data point indicates one biological replicate. Data are presented as mean ± S.D. *p < 0.05, **p < 0.01, ***p < 0.001, and ****p < 0.0001.

Figure 4

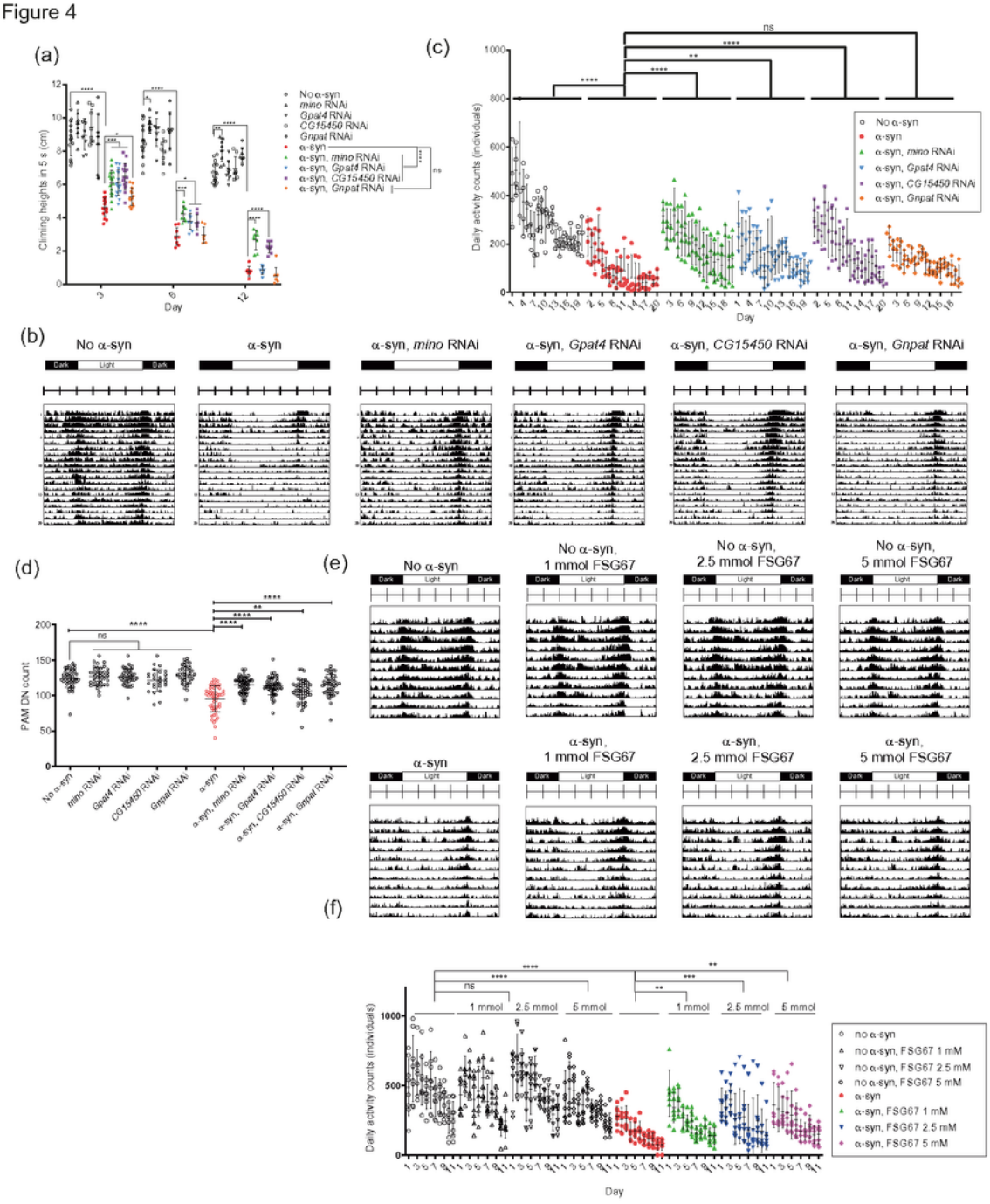

Figure 4

***mino* represents a general GPAT activity in modulating a-syn neurotoxicity.** (**a**) *GPAT* (*mino*, *Gpat4*, *CG15450*) RNAi, but not *Gnpat* RNAi, suppressed the a-syn-induced decline of startle-induced climbing ability in pan-neuronal a-syn-expressing flies (*nSyb-QF2 QUAS-SNCA/+*). *N* = 48, 24, 24, 24, 24, 32, 32, 32, 32, 32, along the order of group list. (**b**, **c**) Mean actograms (**b**) and quantification of daily locomotor activities (**c**) recorded in 12-hour light/dark cycles for flies with pan-neuronal a-syn (*nSyb-QF2 QUAS-*

SNCA/+) and RNAi of GPAT or Gnpat from day 1 onwards. *GPAT* RNAi, but not *Gnpat* RNAi, suppressed the a-syn-induced decline of daily total locomotor activities. (**d**) Quantification of PAM dopaminergic neurons with or without pan-neuronal a-syn-expression (*nSyb-QF2 QUAS-SNCA/+*) and RNAi against *GPAT* or *Gnpat* in flies cultured at 29^{o}C for 3 weeks. *N* = 46, 38, 40, 26, 39, 54, 54, 52, 49, 47, from left to right. (**e**, **f**) Mean actograms (**e**) and quantification of daily locomotor activities (**f**) recorded in 12-hour light/dark cycles for flies with or without pan-neuronal a-syn (*nSyb-QF2 QUAS-SNCA/+*) feed with food supplemented with GPAT inhibitor FSG67 at 1 mmol, 2.5 mmol, 5 mmol or none. *N* = 88, 88, 88, 88, 77, 77, 77, 76, from left to right. Measurements were taken from distinct samples for each timepoint, and were measured repeatedly across timepoints. Data in (**a**) at each timepoint and the data in (**d**) were analyzed with one-way ANOVA followed by Tukey's and Dunnett's multiple comparisons test. The group effects in (**a**, **c**, **f**) were analyzed using two-way ANOVA followed by Tukey's and Dunnett's multiple comparisons test. Each data point indicates one biological replicate from the mean climbing height of 1 vial of 20~30 flies in (**a**). Each data point for one timepoint indicates one biological replicate in (**c**) and (**f**). Data are presented as mean ± S.D. *p < 0.05, **p < 0.01, ***p < 0.001, and ****p < 0.0001.

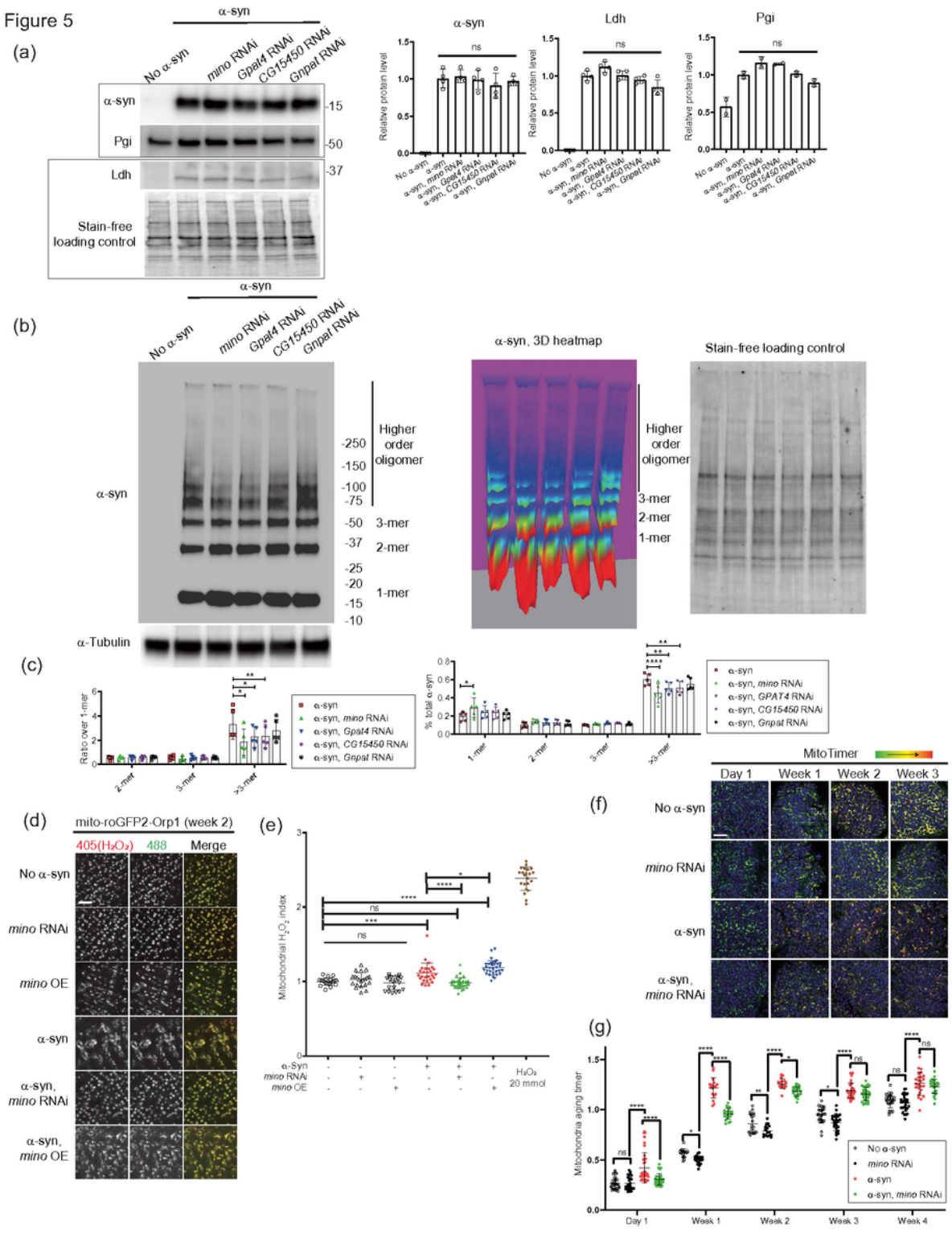

Figure 5

***GPAT* RNAi suppresses a-syn higher-order oligomers formation and mitochondrial ROS accumulation.**

(**a**) *GPAT* RNAi did not affect pan-neuronal a-syn level and a-syn-induced upregulation of glycolysis enzymes Pgi and Ldh. *N* = 4 for a-syn and Ldh, *N* = 2 for Pgi. (**b**) *GPAT* RNAi, but not *Gnpat* RNAi, suppressed the a-syn higher-order oligomers formation. A 3D heatmap of a-syn was shown. (**c**)

Quantification of the ratio between oligomers and monomers, and the percentage of monomers and oligomers to total a-syn in pan-neuronal a-syn-expressing flies (*nSyb-QF2 QUAS-SNCA/+*) with *GPAT* RNAi or *Gnpat* RNAi in (**b**). *N* = 5. (**d**, **e**) *mino* suppressed the elevated mitochondrial ROS in 2-weeks-old flies expressing a-syn in photoreceptor neurons (*Rh1-GAL4/UAS-Mito-roGFP2-Orp1; UAS-SNCA.J7/+*). (**d**) Imaging of mitochondrial H_2O_2 fluorescent sensor (UAS-mito-roGFP2-Orp1) using 405 nm laser for H_2O_2-bound form and 488 nm laser for H_2O_2-free form of the sensor. The H_2O_2 increased as the merged color shift from green to yellow and red. (**e**) Quantification of the ratio between mean intensity in 405 and 488 channels. 20mmol H_2O_2 incubation for 5 mins was used as positive control. (**f**) Green and red channel-merged image and quantification of pan-neuronal MitoTimer in the cortex of optic lobes reflecting the maturation of mitochondria from green to red color. (**g**) Quantification of MitoTimer red-to-green ratio in (**f**). Scale bars represent 5 mm for (**d**) and 10 mm for (**f**). Measurements were taken from distinct samples for each timepoint and also across timepoints. Data in (**a**, **c**, **e**) and each timepoint in (**g**) were analyzed with one-way ANOVA followed by Tukey's and Dunnett's multiple comparisons test. Each data point for one timepoint indicate one biological replicate. Data are presented as mean ± S.D. *p < 0.05, **p < 0.01, ***p < 0.001, and ****p < 0.0001.

Figure 6

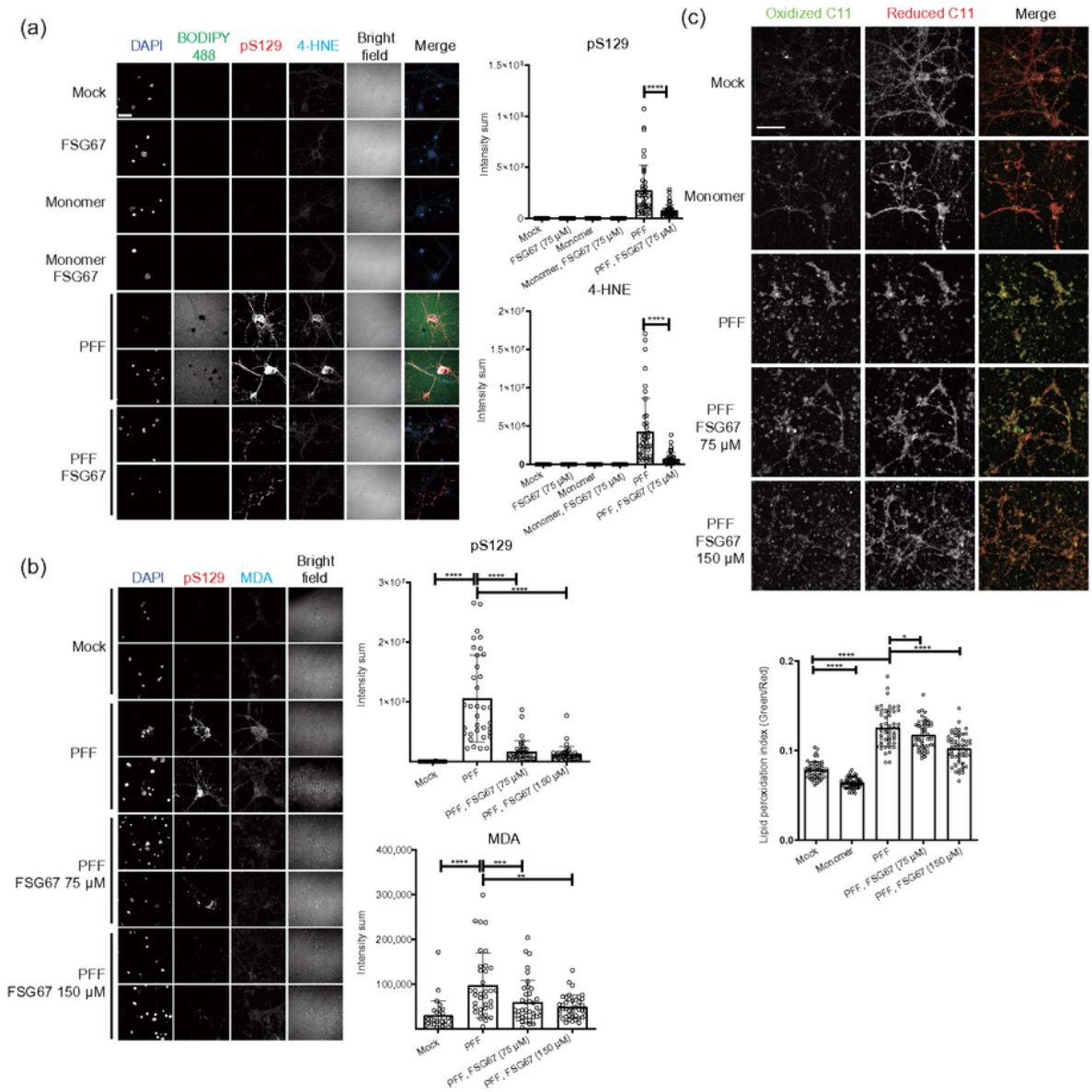

Figure 6

GPAT inhibitor FSG67 suppresses a-syn aggregation propagation and lipid peroxidation product formation in mouse primary neurons transfected with a-syn preformed fibrils (PFF). (**a**) Mouse primary neurons transfected with a-syn monomers or PFF with 75 mmol GPAT inhibitor FSG67 for 2 weeks and stained with BODIPY 488, phosphorylated a-syn pS129 and the lipid peroxidation product 4-HNE. Quantifications of phosphorylated a-syn pS129 and 4-HNE intensity sum for mouse primary neurons

were plotted. Data points are technical replicates from one coverslip; *N* = 34, 32, 36, 36, 41, 43, from left to right. (b) Mouse primary neurons transfected with PFF with 0, 75 or 150 mmol GPAT inhibitor FSG67 for 2 weeks and stained with phosphorylated a-syn pS129 and the lipid peroxidation product MDA. Quantifications of phosphorylated a-syn pS129 and MDA intensity sum for mouse primary neurons were plotted. Data points are technical replicates from one coverslip; *N* = 30, 40, 38, 35, from left to right. (**c**) Mouse primary neurons transfected with PFF with 0, 75 or 150 mmol GPAT inhibitor FSG67 for 4 weeks and live-stained with BODIPY C11 for the lipid peroxidation analysis. Data points are technical replicates from one culture dish; *N* = 51, 54, 48, 51, 57, from left to right. Scale bars represent 30 mm for (**a**) and (**b**), and 80 mm for (**c**). Data were analyzed with one-way ANOVA followed by Tukey's and Dunnett's multiple comparisons test. Each data point indicates one imaged region of cells. Experiments were repeated for two to three times. Data are presented as mean ± S.D. *p < 0.05, **p < 0.01, ***p < 0.001, and ****p < 0.0001.

Supplementary Files

This is a list of supplementary files associated with this preprint. Click to download.

- ncommssourcedata.xlsx
- SupplementaryData1.xlsx
- SupplementaryInformation.pdf
- GraphicalAbstract.png